Weierstraß-Institut
für Angewandte Analysis und Stochastik
Leibniz-Institut im Forschungsverbund Berlin e. V.

Preprint ISSN 2198-5855

Non-instantaneous polarization dynamics in dielectric media

Michael Hofmann[1], Janne Hyyti[2,3], Simon Birkholz[3], Martin Bock[3], Susanta K. Das[3,4], Rüdiger Grunwald[3], Mathias Hoffmann[5], Tamas Nagy[5,6], Ayhan Demircan[5], Marco Jupé[7], Detlev Ristau[7], Uwe Morgner[5,7], Carsten Brée[1], Michael Woerner[3], Thomas Elsaesser[3], Günter Steinmeyer[2,3,*]

submitted: June 3, 2014

[1] Weierstrass Institute
Mohrenstraße 39
10117 Berlin, Germany

[2] Optoelectronics Research Centre
Tampere University of Technology
Korkeakoulunkatu 3
33720 Tampere, Finland

[3] Max-Born-Institut für Nichtlineare Optik und Kurzzeitspektroskopie
Max-Born-Straße 2a
12489 Berlin, Germany

[4] Dept. of Physics
School of Applied Sciences
Campus 3, KIIT University
Bhubaneswar, India 751024

[5] Institut für Quantenoptik
Leibniz-Universität Hannover
Welfengarten 1
30167 Hannover, Germany

[6] Laser-Laboratorium Göttingen e.V.
Hans-Adolf-Krebs-Weg 1
37077 Göttingen, Germany

[7] Laser Zentrum Hannover e.V.
Hollerithallee 8
30419 Hannover, Germany

[*] E-Mail for correspondence:
steinmey@mbi-berlin.de

No. 1961

Berlin 2014

2010 *Physics and Astronomy Classification Scheme.* 42.30.Rx, 78.20.-e, 78.20.Mg, 78.20.Bh.

Key words and phrases. nonlinear optics, ultrafast spectroscopy, interferometric FROG, pulse characterization, time-dependent Schrödinger equation.

Financial support by the Deutsche Forschungsgemeinschaft is gratefully acknowledged (contracts STE 762/9, BR 4654/1, and MO 850/16).

Edited by
Weierstraß-Institut für Angewandte Analysis und Stochastik (WIAS)
Leibniz-Institut im Forschungsverbund Berlin e. V.
Mohrenstraße 39
10117 Berlin
Germany

Fax: +49 30 20372-303
E-Mail: preprint@wias-berlin.de
World Wide Web: http://www.wias-berlin.de/

Abstract

Third-order optical nonlinearities play a vital role for generation[1,2] and characterization[3–5] of some of the shortest optical pulses to date, for optical switching applications[6,7], and for spectroscopy[8,9]. In many cases, nonlinear optical effects are used far off resonance, and then an instantaneous temporal response is expected. Here, we show for the first time resonant frequency-resolved optical gating measurements[10–12] that indicate substantial nonlinear polarization relaxation times up to 6.5 fs in dielectric media, i.e., significantly beyond the shortest pulses directly available from commercial lasers. These effects are among the fastest effects observed in ultrafast spectroscopy. Numerical solutions of the time-dependent Schrödinger equation[13,14] are in excellent agreement with experimental observations. The simulations indicate that pulse generation and characterization in the ultraviolet may be severely affected by this previously unreported effect. Moreover, our approach opens an avenue for application of frequency-resolved optical gating as a highly selective spectroscopic probe in high-field physics.

Third-order optical nonlinearities are a ubiquitous effect in dielectric materials. Under nonresonant conditions outside absorption resonances, they stem from anharmonicities of the binding potential of valence electrons in the material. An oscillating electric field $\mathcal{E}(t)$ induces a dipole moment inside the material, which gives rise to a polarization $P(t) = \epsilon_0 \chi \mathcal{E}(t)$, with the dielectric constant ϵ_0 and the susceptibility χ. In an isotropic medium and under non-resonant conditions, the susceptibility can be written as a series of odd orders of the electric field $P(t) = \epsilon_0 \left(\chi^{(1)} \mathcal{E}(t) + \chi^{(3)} \mathcal{E}^3(t) + \dots \right)$. Assuming an oscillating electric field $\mathcal{E}(t) = E_0 \exp(-i\omega t)$ one therefore expects Fourier components of $P(t)$ at the fundamental frequency ω and all odd harmonics thereof. Using an 800 nm driver pulse, for example, third-harmonic radiation appears in the ultraviolet at 266 nm. Apart from harmonic generation, the real part of $\chi^{(3)}$ nonlinearity also gives rise to a self-effect for the fundamental component, namely self-refraction. This reactive nonlinearity results in a power-dependent phase shift at the driver wavelength. Self-phase modulation is the dominant nonlinear effect in optical fibers. In bulk media, self-refraction additionally induces a spatial lensing effect at high intensities, which is named self-focusing. Both self-phase modulation and self-focusing play a vital role in characterization and generation methods for ultrashort pulses[3,4,15,16]. The pulse generation method of Kerr-lens mode-locking, for example, relies on the quasi-instantaneous action of the self-focusing mechanism. Any delay of the relaxation mechanism of this ultrafast optical switch would severely limit obtainable pulse durations[1,2] from such a laser source. Similarly, one expects incorrect results from any pulse characterization method if a persistence appears in the nonlinear response.

In our experiments, we used an interferometric variant of third-harmonic frequency-resolved optical gating (TH-FROG[4]), see Fig. 1 and Methods section for details. FROG techniques generally measure the spectrally resolved autocorrelation traces of the pulse $E(t)$ under test, i.e., in this case the third-harmonic autocorrelation. Assuming that the nonlinear optical effect employed for the correlation is instantaneous, it is typically possible to unambiguously reconstruct the pulse profile $E(t)$ from the measured FROG trace[12]. The FROG method is fully self-referenced, and no well characterized external reference pulse is required. As interferometric FROG variants allow for a collinear beam path, tight focusing at high numerical apertures enables the use of nanojoule pulses with uncompressed durations of two to three optical cycles as they are

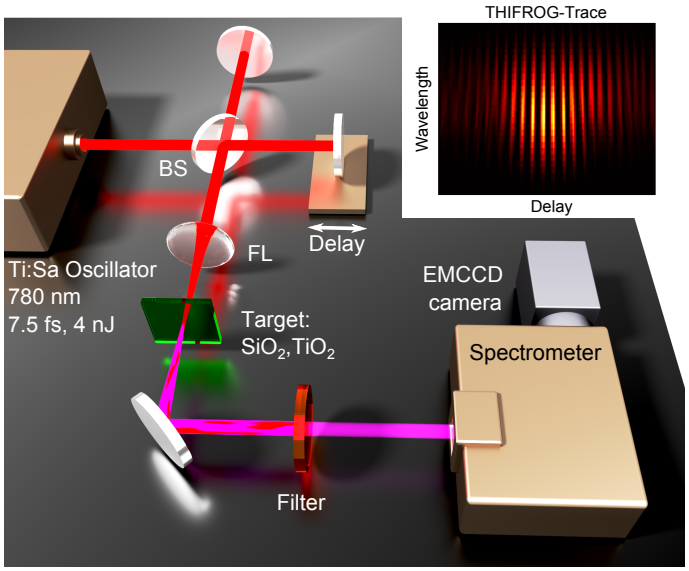

Figure 1 | **Experimental setup.** A few-cycle Ti:sapphire pulse is split into two replicas, one of which experiences an adjustable delay in a Michelson interferometer. After collinear recombination of the replicas, the pulses are focused onto a sample (SiO_2, TiO_2) for the generation of the third harmonic. After suppressing fundamental light with a shortpass filter, the third-harmonic light is spectrally dispersed in a spectrometer. The light is detected with an intensified CCD camera. The resulting interferometric FROG traces exhibit interference patterns at the fundamental wavelength and its harmonics, see inset.

directly available from mode-locked oscillators[1,2]. Using 7.5 fs pulses at 800 nm center wavelength, we measured interferometric TH-FROG traces in two different nonlinear optical $\chi^{(3)}$ materials, namely silica SiO_2 and titania TiO_2. Experimental results are displayed in Fig. 2. Even without pulse retrieval, one can immediately see that the titania-based FROG trace is significantly wider than the one measured in silica. This broadening effect becomes even more pronounced in a comparison of the reconstructed electric-field profiles in Fig. 2(d,h). Despite of an otherwise completely identical setup, a pulse duration of 10.1 fs (FWHM) is retrieved for silica, whereas the use of titania yields 15.7 fs. Deviations between the retrieved pulse durations and the input pulse duration of 7.5 fs may partially stem from imperfections in the dispersion compensation as well as from unavoidable spatial aberrations of the tight focusing geometry[17]. Following the approach described in Ref. 11, we deconvolved the titania trace with a single-sided exponential kernel, yielding a relaxation time constant of 6.5 fs [Fig. 3]. This effect was reproduced in a series of measurements on different samples that were manufactured by different deposition methods.

The peak intensity of the 800 nm pulses reaches values of the order of 0.1 TW/cm^2 on the samples. As a result, free electrons and holes are excited via two- and three-photon interband transitions in the titania sample. From the respective absorption coefficients reported in Ref. 18, one estimates a free carrier density of several 10^{17} cm^{-3}. Under such conditions, both nonlinear inter- and intraband polarizations occur and — in general — the related (imaginary or real) inter- and intraband currents represent source terms for generating electric fields at new frequencies. An analysis of this scenario requires in-depth calculations of the nonlinear response which are presented next.

In our theory, we numerically solved the time-dependent Schrödinger equation, see Methods section for details. We employed pseudopotentials[14] that correctly describe the effective mass

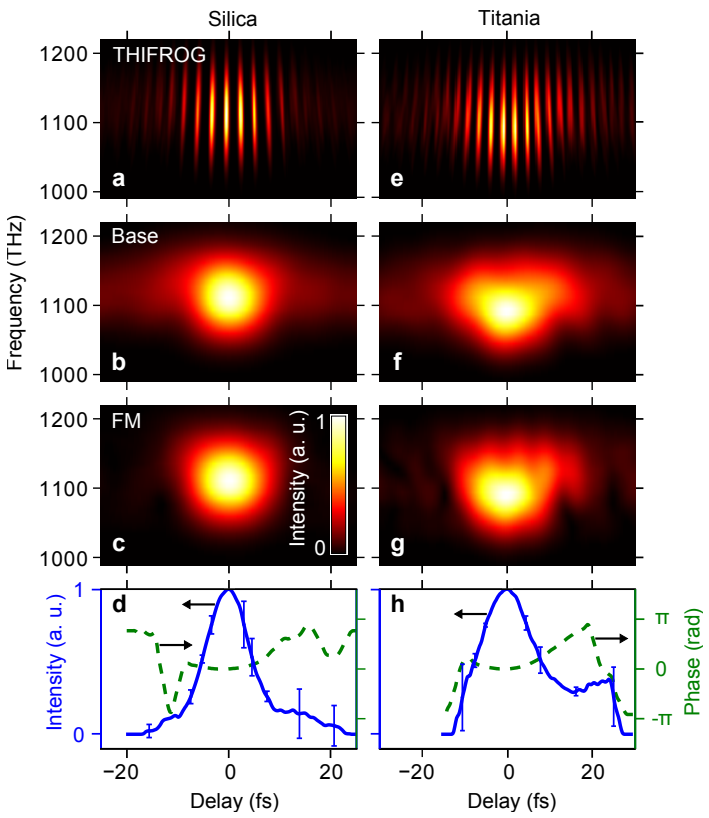

Figure 2 | Experimental results. a – d As measured with SiO_2 and **e – h** with TiO_2. **a, e** Originally measured interferometric third-harmonic FROG traces. Experimental conditions are identical except for the nonlinear material. **b, f** Resulting base bands obtained by Fourier filtering. Fringe frequencies higher than $0.5\lambda_0^{-1}$ are suppressed ($\lambda_0 = 800$ nm). **c, g** Fundamental modulation side band at fringe frequency λ_0^{-1}. Frequencies below $0.5\lambda_0^{-1}$ and above $1.5\lambda_0^{-1}$ have been suppressed. The squared moduli of the rapidly oscillating fields are shown, i.e., intensities. **d, h** Retrieved intensities (blue lines) and phases (dashed green lines). Error bars have been computed from the standard deviation of several independent retrievals.

of the valence electrons and also yield the correct bandgap of the respective dielectric material. The calculations show that the nonlinear response is dominated by nonlinear interband polarization whereas intraband contributions play a minor role. In titania, the intraband current amplitudes are typically one order of magnitude smaller than the interband contributions. Results of the calculations are summarized in Fig. 4. Silica exhibits a bandgap of 9 eV. Therefore, the third harmonic of the 1.5 eV excitation is still off-resonant. In this case, the polarization follows the rapidly oscillating fundamental field $\mathcal{E}(t)$ [Fig. 4(a)]. Polarization contributions at the third harmonic $\propto \mathcal{E}^3(t)$ are comparatively weak [Fig. 4(e)]. For titania with a bandgap of ≈ 3.2 eV, the third harmonic becomes resonant with the quantum mechanical dipole, cf. Fig. 4(c). This gives rise to a apparent build-up of an oscillation of P at the third harmonic frequency [Fig. 4(a)]. The spectral overlap causes a continuation of the dipole oscillation for several cycles beyond the excitation pulse. It is important to convince oneself that the resulting dynamics stems chiefly from interband transitions, see Fig. 4(d). Deconvolving the computed titania response with a single-sided exponential, we again determine a relaxation time constant of 8 fs [Fig. 4(e)], in remarkable proximity to the measured values. Isolating the fundamental frequency contribution of the polarization and comparing its phase to the driver field, one can also extract the self-refraction part of the response. Here one observes a qualitatively similar behavior as for the third

harmonic. Quite generally, once there is a response in resonance with the quantum mechanical dipole, self-phase modulation and self-focusing will not immediately follow the envelope of the driver pulse anymore, but show a persistence of several femtoseconds beyond [Fig. 4(f)]. At constant bandgap, the effective mass in the pseudopotential plays a decisive role for the length of the observed relaxation time constant, i.e., the relaxation behavior on few-femtosecond time scales may be used as a local probe for the effective mass of the valence electrons inside the material. Moreover, we repeated the simulations assuming hydrogenlike atomic potentials[13] and observed qualitatively the same behavior. Once there is spectral overlap between the third harmonic and the conduction band, a prominent persistence of the nonlinear susceptibility is observed.

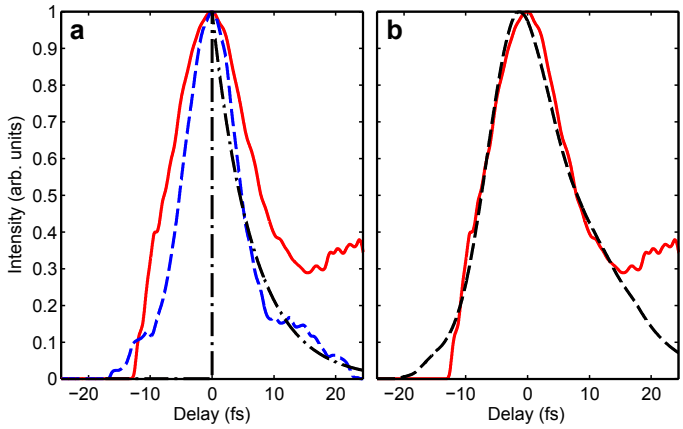

Figure 3 | Deconvolution analysis. a Solid red curve: measured intensity profile using TiO_2. Dashed blue curve: same using SiO_2. Dash-dotted black curve: single-sided exponential convolution kernel $R(t)$, cf. Eq. (2) in the Methods section. $1/e$ polarization decay time is 6.5 fs. **b** Solid red curve: same as in **a**. Dashed black curve: convolved silica trace $I_{SiO_2} * R$ yielding the best agreement with I_{TiO_2} in the range from -10 to 10 fs.

In principle, these findings can also be qualitatively understood in a semi-classical picture, as previously discussed for nano-plasmonic systems[11]. Driving a harmonic oscillator far off resonance, the forced oscillation will immediately disappear if the driver is switched off. On resonance, however, the forced oscillation will persist for several cycles, before the energy of the oscillating system is depleted due to emission of an electromagnetic wave. In this scenario, the intrinsic single-sided exponential decay of the system gives rise to Lorentzian line shapes. Moreover, in a weakly anharmonic oscillator, there may be a build-up of a resonant oscillation if the system is driven at a suitable subharmonic. Quickly switching off the driver, one then also observes a persistence of the resonant oscillation. Despite of the intriguing accessibility of such models, however, semi-classical pictures fail to correctly predict the sharp transition between resonant and off-resonant excitation, which is only correctly modeled in the full quantum mechanical simulations.

Our findings have important implications for applications of nonlinear $\chi^{(3)}$ effects, in particular for short-pulse characterization techniques. Specifically, limitations arise when the third harmonic approaches the band gap of the nonlinear material. While this appears straightforward for third-harmonic generation, adverse effects also appear at the fundamental wavelength for self-refraction, see the tail of the $\chi^{(1)}$ contribution in Fig. 4(c). This modified response could, in principle, limit Kerr-lens mode-locking, even though we are not aware of such lasers being operated above one third of the bandgap[19–21]. More importantly, our findings impose limitations on $\chi^{(3)}$ based pulse measurement techniques in the visible and ultraviolet range. Using sapphire or

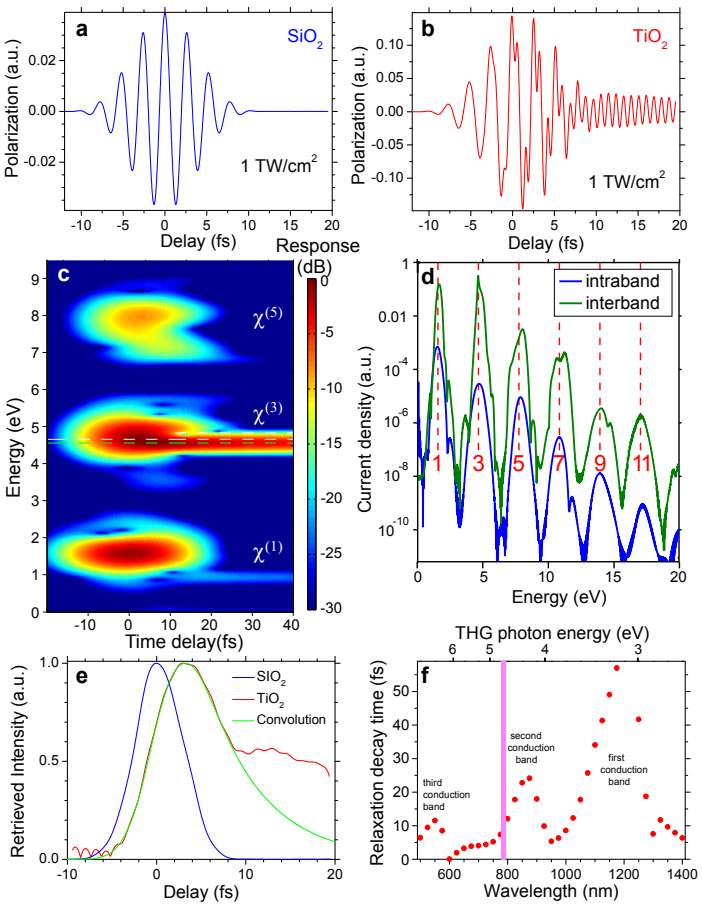

Figure 4 | Solutions of the time-dependent Schrödinger equation. a Computed polarization response for SiO_2. Intensity 1 TW/cm^2. **b** Same for TiO_2. **c** Temporally gated spectrograms of the polarization for TiO_2. Resonant behavior is clearly identified by a lasting response at a given frequency. **d** Spectrally resolved interband (green curve) and intraband (blue curve) current densities, cf. Methods section and Refs. 28,29. Intraband currents mostly originate from first and second conduction band. Positions of fundamental and all odd harmonics are indicated by dashed red lines. Interband contributions to the observed nonlinearities clearly overrule intraband effects. **e** Deconvolution analysis, cf. Methods section. Simulated intensity profile $|E_{\mathrm{THG}}(t)|^2$ for use of SiO_2 (blue) is compared to TiO_2 (red). Convolving the titania profile with a single-sided exponential with relaxation time constant $\tau_{\mathrm{pol}} = 8$ fs yields a good approximation to the TiO_2 profile for $t = -10$ to $+10$ fs. **f** Systematic scan of excitation wavelength with subsequent deconvolution analysis. The resulting τ_{pol} shows a strong reaction to an overlap of the third harmonic of the excitation wavelength with various conduction bands. The third harmonic of the excitation wavelength is in resonance with the second conduction band of TiO_2. The pink band indicates the central excitation wavelength.

silica as the medium, limitations may appear below 600 nm. There is an increasing trend to employ near-resonant thin-film samples[22–24], as they provide substantially enhanced conversion efficiencies. This favorable behavior may come with a significant loss of temporal resolution, particularly for pulses in the few-cycle regime. Finally, even using the widest bandgap material LiF, sensible $\chi^{(3)}$ based characterization appears to be restricted to wavelengths above 320 nm.

In conclusion, we present a novel approach of using frequency-resolved optical gating as a tool to resolve the temporal response of nonlinear optical processes at a few-cycle time scale. Essentially, our method probes the effective mass of valence electrons and shows a threshold-like behavior on the bandgap material. The reported polarization decay times of ≈ 7 fs belong to the fastest non-instantaneous effects that were ever reported at near-visible wavelengths. Our findings may have important effects in ultrafast optics, imposing the avoidance of resonant three-photon effects for sensible characterization and passive mode-locking techniques in the few-cycle regime. Given that this issue is apparently not restricted to solid-state materials, there may also be consequences for attosecond pulse characterization techniques[25]. In a somewhat simplifying fashion, particular care appears advisable whenever odd harmonics become resonant with resonant transitions and if pulse durations are below ten cycles of the carrier field. Considering that the shortest attosecond pulses to date[25] are approaching the single-cycle regime, there may be an incentive to prefer spectral-interferometry based techniques over correlation techniques in this regime. Despite all the apparent possible limitations, our new method opens a new avenue for accessing fundamental parameters of a dielectric material by an optical probe technique.

Methods

Measurements. For the measurements, we employed a setup that is widely identical to the one described in Ref. 22, cf. Fig. 1. The input pulses from a Ti:sapphire laser (7.5 fs pulse duration, 800 nm center wavelength) are split into two beam paths, experience a relative delay, and are then collinearly recombined and focused into the $\chi^{(3)}$ material by an $f = 25$ mm concave mirror. Dispersion of the beam splitter setup and the air paths is precompensated by chirped mirrors. The generated third-harmonic light is recollimated by a UV microscope objective. Fundamental light is rejected by two interference filters, which transmit a 40 nm bandwidth at 266 nm center wavelength. The light is then spectrally dispersed in a spectrograph equipped with an electron multiplier charge coupled device (EMCCD). The experiments employed titania thin-film samples that are deposited on silica substrates. These samples were oriented with the titania side towards the concave mirror. Reference measurements were done in the same geometry, using the surface third-harmonic generation of silica substrates.

Retrieval. The measured interferometric FROG traces are of the form

$$I_{\text{THIFROG}}(\omega,\tau) \propto \left| \int_{-\infty}^{+\infty} \left(\mathcal{E}(t) + \mathcal{E}(t-\tau)\right)^3 \exp\left(-i\omega t\right) \mathrm{d}t \right|^2 , \tag{1}$$

where τ is the delay between the two correlator arms, ω the angular optical frequency, and $\mathcal{E}(t) = E(t)\exp(i\omega_0 t)$ the rapidly oscillating electric field at carrier frequency ω_0. Measured example traces are shown in Figs. 2 (a, e). Using Fourier analysis, this measured FROG trace

can be decomposed into three subtraces $I^{(n)}_{\text{THIFROG}}(\omega,\tau)$ that show sinusoidal variation with $n\omega\tau$, $(n=1\ldots3)$ and a fourth subtrace ($n=0$) that does not rapidly vary with delay[10]. Examples for $n=0$ and 1 are shown in Figs. 2 (b, f) and (c, g), respectively. In principle, one can retrieve the complex-valued $E(t)$ from any of the three subtraces $I^{(n)}_{\text{THIFROG}}(\omega,\tau)$ ($n=0\ldots2$) whereas the trace for $n=3$ contains only a spectral interferometry signal. Moreover, given the fairly weak signals, one could practically only use the subtraces for $n=0$ and 1 for retrieval of $E(t)$. To this end, a specialized retrieval software was written that computes $I_{\text{THIFROG}}(\omega,\tau)$ via Eq. (1) for a given initial guess for $E(t)$, separates the relevant subtraces, and employs the Nelder-Mead optimization algorithm to iteratively minimize the difference between measured and computed FROG trace. In this iterative construction, the delay range encompassed a total of 80 fs with a total of 50 points to represent $E(t)$. This corresponds to a temporal resolution of 1.6 fs, i.e., 70% of the optical cycle at 800 nm. Retrieval was seeded with assumption of an unchirped hyperbolic secant pulse shape, with a width that was matched to the autocorrelation width of the $I^{(0)}_{\text{THIFROG}}$ component. Using the redundancy in the THIFROG traces, a total of three independent retrieval attempts were made for each data set, employing either the $I^{(0)}_{\text{THIFROG}}$ or the $I^{(1)}_{\text{THIFROG}}$ component as well as a combination of the two. These independent retrievals were employed for an estimation of the robustness of the retrieved pulse shapes, see error bars in Figs. 2 (d, h).

Deconvolution. For deconvolution analysis of the traces, we iteratively reconstruct the response function $R(t)$ that minimizes the functional distance

$$\epsilon(t)=\left|I_{\text{TiO}_2}(t)-\int_0^\infty I_{\text{SiO}_2}(t-t')R(t')dt'\right|^2. \tag{2}$$

in a certain delay range. For Fig. 2(d,h), $-10\,\text{fs} < t < 10\,\text{fs}$ was chosen. The intensities $I_{\text{X}}(t)=|\mathcal{E}_{\text{X}}(t)|^2$, $\text{X}=\text{SiO}_2,\text{TiO}_2$ are deduced from the interferometric FROG measurements at the silica and titania samples, respectively. The response function $R(t)$ is defined as single-sided exponential $R(t)=\exp\left(-t/\tau_{\text{pol}}\right)$, with τ_{pol} being the polarization decay time. The deconvolution is again computed in a forward fashion, starting with an initial guess for τ_{pol}. Numerically minimizing Eq. (2), we use again Nelder-Mead optimization for the deconvolution procedure. For deconvolving the theoretically computed polarization [Fig. 4(d)], we employed the identical procedure.

Time-dependent Schrödinger equation. For the numerical analysis, we use the single-active-electron approximation with the 1D pseudopotential

$$U(r)=\sum_{n=-\infty}^{\infty} c_1\left(\tanh^2(c_2(r+na))-1\right)+c_3\left(\tanh^4(c_2(r+na))-1\right). \tag{3}$$

For silica, we use the values from Ref. 14, i.e., $a=5.4$ Å, $c_1=54.86$ eV, $c_2=1.553\,\text{Å}^{-1}$, and $c_3=0$, yielding a bandgap $E_{\text{g}}=9$ eV and an effective mass $m^*=0.4m_e$ in the lowest conduction band. For modeling the effective mass $m^*\approx m_e$ and band gap $E_{\text{g}}=3.2$ eV of the anatase modification of TiO_2[26], a simple $\tanh^2$ functional dependence in Eq. (3) was found insufficient. Adding a $\tanh^4$ term and using $a=9.51$ Å, $c_1=c_3=31.31$ eV, and

$c_2 = 2.598\,\text{Å}^{-1}$, we obtain a good match for the pseudopotential of titania, yet with a slightly smaller effective mass $m^* = 0.61\,m_e$ than experimentally reported.

Second, to simulate the interaction with the laser pulse, we consider the time-dependent Schrödinger equation (TDSE)

$$i\hbar\frac{\partial}{\partial t}\psi_k(t) = \left(H_0 + \frac{e}{m_e}A(t)p\right)\psi_k(t), \tag{4}$$

where H_0 is the Hamiltonian of the stationary problem, $A(t)$ is the vector potential of the laser field and $\psi_k(t)$ is a superposition of one-electron Bloch waves with quasimomentum k. As initial condition, we assume fully occupied valence bands and solve the TDSE for one localized single-electron in each valence band and every k-state independently[27]. The macroscopic current density is then computed as the sum over all k-states and all valence bands.

The formalism was used to model interband transitions from the valence band into the first thirteen conduction bands as well as intra conduction band transitions. For an estimation of the prevalent mechanism, all intraband currents were summed up and compared to the total interband current[28,29].

In the numerical simulations, a $\cos^4$ excitation pulse shape[27] with 6.5 fs full width at half maximum was assumed to temporally localize the response. $\lambda_0 = 800\,\text{nm}$ (1.55 eV) was assumed as central excitation wavelength.

Author contributions M. Hofmann and J.H. contributed equally to this work. Thin-film TiO_2 samples were provided by M.J. and D.R. M.B., S.K.D., and R.G. performed the TH-FROG measurements. M. Hofmann, and C.B. numerically solved the time-dependent Schrödinger equation. T.E. and M.W. interpreted the results. J.H. wrote the FROG retrieval software. Experimental results have been analyzed by J.H., S.B., M. Hoffmann, T.N., A.D., T.E., U.M., and G.S. All authors contributed to the manuscript.

Competing financial interest The authors declare that they have no competing financial interests.

Correspondence Correspondence and requests for materials should be addressed to G.S. (email: steinmey@mbi-berlin.de).

References

[1] Steinmeyer, G., Sutter, D. H., Gallmann, L., Matuschek, N. & Keller, U. Frontiers in Ultrashort Pulse Generation: Pushing the Limits in Linear and Nonlinear Optics. *Science* **286**, 1507–1512 (1999).

[2] Morgner, U., Kärtner, F. X., Cho, S. H., Chen, Y., Haus, H. A., Fujimoto, J. G., Ippen, E. P., Scheuer, V., Angelow, G. & Tschudi, T. Sub-two-cycle pulses from a Kerr-lens mode-locked Ti:sapphire laser. *Opt. Lett.* **24**, 411–413 (1999).

[3] Kane, D. J. & Trebino, R. Characterization of arbitrary femtosecond pulses using frequency-resolved optical gating. *IEEE J. Quantum Electron.* **29**, 571 (1993).

[4] Tsang, T., Krumbügel, M. A., DeLong, K. W., Fittinghoff, D. N. & Trebino, R. Frequency-resolved optical-gating measurements of ultrashort pulses using surface third-harmonic generation. *Opt. Lett.* **21**, 1381–1383 (1996).

[5] Pasquazi, A., Peccianti, M., Park, Y., Little, B. E., Chu, S. T., Morandotti, R., Azaña, J. & Moss, D. J. Sub-picosecond phase-sensitive optical pulse characterization on a chip *Nature Photon.* **5**, 618−623 (2011).

[6] Vlasov, Y., Green, W. M. J. & Xia, F. *Nature Photon.* **2**, 242–246 (2008).

[7] Demircan, A., Amiranashvili, S. & Steinmeyer, G. Controlling Light by Light with an Optical Event Horizon. *Phys. Rev. Lett.* **106** 163901 (2011).

[8] M. Rentzepis, M. R. Topp, R. P. Jones, and J. Jortner, Picosecond Emission Spectroscopy of Homogeneously Broadened, Electronically Excited Molecular States. *Phys. Rev. Lett.* **25**, 1742−1745 (1970).

[9] J. Takeda, K. Nakajima, S. Kurita, S. Tomimoto, S. Saito, and T. Suemoto. Time-resolved luminescence spectroscopy by the optical Kerr-gate method applicable to ultrafast relaxation processes. *Phys. Rev. B* **62**, 10083−10087 (2000).

[10] Stibenz, G. & Steinmeyer, G. Interferometric frequency-resolved optical gating. *Opt. Express* **13**, 2617–2626 (2005).

[11] Anderson, A., Deryckx, K. S., Xu, X. G., Steinmeyer, G. & Raschke, M. B. Few-Femtosecond Plasmon Dephasing of a Single Metallic Nanostructure from Optical Response Function Reconstruction by Interferometric Frequency Resolved Optical Gating. *Nano Lett.* **10**, 2519−2524 (2010).

[12] Trebino, R. *Frequency-Resolved Optical Gating: The Measurement of Ultrashort Laser Pulses*, (Springer, 2002).

[13] Muller, H. G. An efficient propagation scheme for the time-dependent Schrödinger equation in the velocity gauge. *Laser Phys.* **9**, 138148 (1999).

[14] Paasch-Colberg, T., Schiffrin, A., Karpowicz, N., Kruchinin, S., Sağlam, Ö., Keiber, S., Razskazovskaya, O., Mühlbrandt, S., Alnaser, A., Kübel, M., Apalkov, V., Gerster, D., Reichert, J., Wittmann, T., Barth, J. V., Stockman, M. I., Ernstorfer, R., Yakovlev, V. S., Kienberger, R. & Krausz, F. Solid-state light-phase detector. *Nature Photon.* **8**, 214−218 (2014).

[15] Meshulach, D., Barad, Y. & Silberberg, Y. Measurement of ultrashort optical pulses by third-harmonic generation. *J. Opt. Soc. Am. B* **14**, 2122−2125 (1997).

[16] Major, A., Yoshino, F., Aitchison, J. S. & Smith, P. W. E. Wide spectral range third-order autocorrelator based on ultrafast nonresonant nonlinear refraction. *Opt. Lett.* **29**, 1945−1947 (2004).

[17] Amir, W., Planchon, T. A., Durfee, C. G., Squier, J. A., Gabolde, P., Trebino, R. & Müller, M. Simultaneous visualization of spatial and chromatic aberrations by two-dimensional Fourier transform spectral interferometry. *Opt Lett.* **31**, 2927−2929 (2006).

[18] Evans, C. C., Bradley, J. D. B., Martí-Panameño, E. A. & Mazur, E. Mixed two- and three-photon absorption in bulk rutile (TiO_2) around 800 nm. *Opt. Express* **20**, 3118–3128 (2012).

[19] Uemura, S. & Torizuka, K. Generation of 12-fs pulses from a diode-pumped Kerr-lens mode-locked Cr:LiSAF laser. *Opt. Lett.* **24**, 780−782 (1999).

[20] Zhao, H. & Major, A. Powerful 67 fs Kerr-lens mode-locked prismless Yb:KGW oscillator. *Opt. Express* **21**, 31846−31851 (2013).

[21] Tolstik, N., Sorokin, E. & Sorokina, I. T. Kerr-lens mode-locked Cr:ZnS laser. *Opt. Lett.* **38**, 299−301 (2013).

[22] Das, S. K., Schwanke, C., Pfuch, A., Seeber, W., Bock, M., Steinmeyer, G., Elsaesser, T., Grunwald, R. Highly efficient THG in TiO2 nanolayers for third-order pulse characterization. *Opt. Express* **19**, 16985−16995 (2011).

[23] Djurisic, A. B. & Leung, Y. H. Optical properties of ZnO nanostructures. *Small* **2**, 944−961.

[24] Chen, A., Yang, G., Long, H., Li, F., Li, Y. & Lu, P. Nonlinear optical properties of laser deposited CuO thin films. *Thin Solid Films* **517**, 4277−4280 (2009).

[25] Chini, M., Zhao, K. & Chang, Z. The generation, characterization and applications of broadband isolated attosecond pulses. *Nature Photon.* **8**, 178−186 (2014).

[26] Tang, H., Prasad, K., Sanjinès, R., Schmid, P. E. & Lévy, F. Electrical and optical properties of TiO2 anatase thin films. *J. Appl. Phys.* **75**, 2042−2047 (1994).

[27] Korbman, M., Kruchinin, S. Y. & Yakovlev, V. S. Quantum beats in the polarization response of a dielectric to intense few-cycle laser pulses. *New J. Phys.* **15**, 013006 (2013).

[28] Juvé, V., Holtz, M., Zamponi, F., Woerner, M., Elsaesser, T. & Borgschulte, A. Field-Driven Dynamics of Correlated Electrons in LiH and $NaBH_4$ Revealed by Femtosecond X-Ray Diffraction. *Phys. Rev. Lett.* **111**, 217401 (2013).

[29] Somma, C., Reimann, K., Flytzanis, C., Elsaesser, T. & and Woerner, M. High-Field Terahertz Bulk Photovoltaic Effect in Lithium Niobate. *Phys. Rev. Lett.* **112**, 146602 (2014).